ONLINE FIRST March 23, 2026

Computer Assisted Methods in Engineering and Science
***, https://doi.org/10.24423/cames.2026.1874

Isogeometric Topology Optimization Based on Topological Derivatives*)

Guilherme Henrique TEIXEIRA[1)*], Nepomuk KRENN[2)], Peter GANGL[2)], Benjamin MARUSSIG[1)]

[1)] *Graz University of Technology, Institute of Applied Mechanics, Graz, Austria*
[2)] *Johann Radon Institute for Computational and Applied Mathematics, Linz, Austria*

[*] *Corresponding Author: teixeira@tugraz.at*

Topology optimization is a valuable tool in engineering, facilitating the design of optimized structures. However, topological changes often require a remeshing step, which can become challenging. In this work, we propose an isogeometric approach to topology optimization driven by topological derivatives. The combination of a level-set method together with an immersed isogeometric framework allows seamless geometry updates without the necessity of remeshing. At the same time, topological derivatives provide topological modifications without the need to define initial holes [7]. We investigate the influence of higher-degree basis functions in both the level-set representation and the approximation of the solution. Two numerical examples demonstrate the proposed approach, showing that employing higher-degree basis functions for approximating the solution improves accuracy, while linear basis functions remain sufficient for the level-set function representation.

Keywords: topology optimization, isogeometric analysis, topological derivatives, level-set method, immersed methods, higher-degree basis function.

1. Introduction

Design optimization describes an iterative process to define the optimal geometry of a structure given some constraints. This problem can be approached in several ways, including the optimization of geometric parameters, such as radius, length, or width (Fig. 1a), the boundaries of the shape (Fig. 1b) [46], or the material distribution of the structure (Fig. 1c) [26]. The last one is known as topology optimization, and since it was first introduced in [9], several methods

*) The results of this study were presented at GAMM 2025 – 95th Annual Meeting of the International Association of Applied Mathematics and Mechanics, April 7–11, 2025, Poznań, Poland.

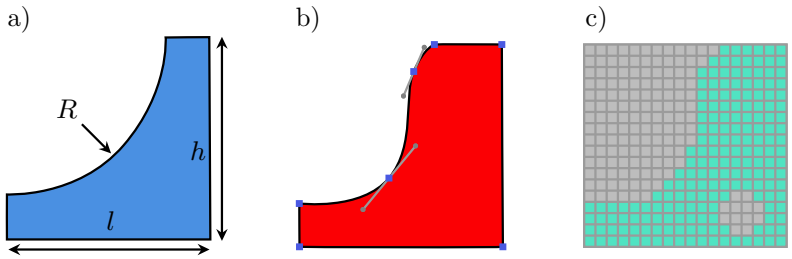

Fig. 1. Different types of optimization: a) parameter optimization, b) shape optimization, c) topology optimization.

have been developed to approach the problem, and as a consequence, various challenges have been addressed [36]. The most popular classes of topology optimization methods are based on design representations by means of density or level-set functions.

Density-based approaches, widely used in topology optimization [36], represent the design through a density variable equal to 1 for material and 0 for void. These methods can be used on a fixed background mesh on which the density variable is defined element-wise, identifying whether an element is solid or void, thereby avoiding the need for remeshing during the optimization process. However, a well-known challenge of density-based topology optimization is the presence of unphysical intermediate materials. This issue is overcome through penalization techniques, such as the solid isotropic material with penalization (SIMP), removing gray areas and resulting in nearly black-and-white designs [13].

In level-set-based approaches [29], the material distribution is represented by the sign of a continuous level-set function which evolves in the course of the optimization process. Level- set methods have been extensively applied to shape and topology optimization, either coupled with a remeshing strategy [15] or applied on a fixed background mesh [2, 3, 44]. The evolution of the level-set function is guided either by shape derivatives via a Hamilton–Jacobi transport equation [2] or by topological derivatives [7]. In the former case, the resulting design heavily depends on the initial topology. New holes cannot be directly introduced, as the method relies on the holes in the initial geometry, which can then be merged or cancelled in the optimization process. In order to allow for the nucleation of new holes, the method has been coupled with topological derivatives in [1, 10]. Another possible approach combining the level-set method and topological derivatives without solving the Hamilton–Jacobi is proposed in [7], with many applications reported in the literature [8, 11, 16, 25, 27, 28, 47] and has also been extended to multi-material problems in [17]. In this algorithm, the optimization is guided only by the topological derivative.

Isogeometric analysis (IGA), first introduced in [21], presents the concept of connecting design and analysis using the same B-splines representing the geometry as basis functions. The straightforward control over the degree and smoothness of a B-spline basis is quite valuable for numerical simulations. Several research studies have been conducted using the isogeometric concept in various topology optimization approaches. On the one hand, applications of the density method in the context of IGA have been reported in several studies in the literature [20], where a connection between the optimization and the CAD environments [34], as well as the benefits of refinement schemes, are straightforwardly targeted into the approach [38, 42]. On the other hand, the conventional level-set method has been used with different discretizations for the level-set function, such as radial basis functions [4, 35], B-splines [22], or piecewise constant functions [23]. To the best of our knowledge, the combination of IGA and topological-derivative-based level-set optimization has only been considered in [30], where the conventional shape-derivative-based level-set method extended by a topological derivative term was used.

In this work, we apply the approach of [7] within the isogeometric framework, using B-splines both for the level-set function discretization and as basis functions to approximate the solution. Compared to standard level-set methods, this approach has the following advantages. Since it uses a fixed background mesh, it eliminates the need for remeshing, and, by using the topological derivative to guide the evolution of the level-set function, it also removes the necessity of defining initial holes and does not require solving the Hamilton–Jacobi equation, relying only on the topological derivative to guide the evolution of the level-set function. In addition, compared to standard density-based methods, this approach does not introduce artificial intermediate materials, since it uses a level-set function to describe the design.

Our contribution focuses on the combination of the level-set method, topological derivatives, and IGA, providing initial configurations free from geometric approximation errors and a simplified fixed high-degree background mesh defined by the knot vector and control points, which also allows straightforward higher-degree simulations. One challenge to this approach is the handling of the material interface, since we use a fixed mesh that does not adapt to the level-set function. We study the sensitivity of the level-set representation in the optimized topology due to different polynomial degrees used for approximating the level-set function and the solution. To accomplish this, we investigate two different settings: one with the same polynomial degree for both approximations, and another one with a linear level-set function discretization and a higher-degree approximation of the solution.

Therefore, in Sec. 2, we present the linear elasticity problem investigated in the topology optimization approach and the main considerations for applying

IGA to it. Then, the definition of the level-set function and the derived topological derivative are provided in Secs. 3 and 4, respectively. In addition, Sec. 5 addresses the procedures for dealing with the cut elements, and two numerical results applied to linear elasticity problems are shown in Sec. 6. Finally, in the conclusion, we summarize the main findings of the numerical examples.

2. Problem description

In this section, we present an overview of the problem to which our approach is applied. The problem studied is the compliance minimization in two-dimensional linear elasticity, and here we present the governing equation, the formulation of the minimization problem, and the key considerations for applying IGA using an immersed approach based on the level-set method.

2.1. Linear elasticity problem

In this work, we consider linear elasticity problems defined on a domain Ω, where the boundary $\partial\Omega$ is divided into three disjoint parts, such that $\Gamma_D \cap \Gamma_N = \emptyset$, $\Gamma_D \cap \Gamma_0 = \emptyset$, $\Gamma_N \cap \Gamma_0 = \emptyset$ and $\Gamma_D \cap \Gamma_N \cap \Gamma_0 = \emptyset$, as shown in Fig. 2a. On these three parts of the boundary, Dirichlet boundary conditions are applied on Γ_D, Neumann boundary conditions in Γ_N, and zero Neumann boundary conditions are applied on Γ_0. Therefore, the governing equations for the problem are given by:

$$\begin{cases} -\nabla \cdot (\boldsymbol{\sigma}(\mathbf{u})) = \mathbf{0} & \text{in } \Omega, \\ \mathbf{u} = \mathbf{0} & \text{on } \Gamma_D, \\ \boldsymbol{\sigma}(\mathbf{u}) \cdot \mathbf{n} = \boldsymbol{\tau} & \text{on } \Gamma_N, \\ \boldsymbol{\sigma}(\mathbf{u}) \cdot \mathbf{n} = \mathbf{0} & \text{on } \Gamma_0. \end{cases} \tag{1}$$

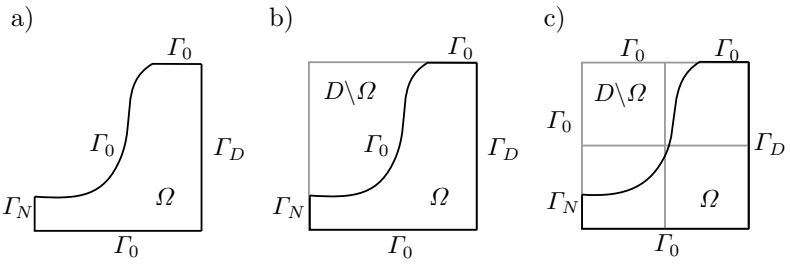

Fig. 2. Representation of the domain problem: a) domain Ω defined by the level-set function, b) domain Ω as a subset of domain D, c) domain Ω inside a B-spline background mesh defined by the knot vector of the geometry D.

Here, $\boldsymbol{\tau}$ is the load applied on the boundaries and $\mathbf{n}$ is the normal vector on them. In addition, $\mathbf{u}$ represents the displacement field and $\boldsymbol{\sigma}$ is the stress tensor, which, for linear elasticity and isotropic materials, is defined as

$$\boldsymbol{\sigma}(\mathbf{u}) = 2\mu\boldsymbol{\epsilon}(\mathbf{u}) + \lambda \operatorname{tr}(\boldsymbol{\epsilon}(\mathbf{u}))\mathbf{I},$$

where

$$\boldsymbol{\epsilon}(\mathbf{u}) = \frac{1}{2}\left(\nabla\mathbf{u} + (\nabla\mathbf{u})^T\right)$$

is the strain tensor and, for 2D plane strain,

$$\mu = \frac{E}{2(1+\nu)}, \qquad \lambda = \frac{E\nu}{(1+\nu)(1-2\nu)}$$

are the Lamé parameters, written in terms of Young's modulus E and Poisson's ratio ν.

In this scenario, the domain Ω represents the material distribution of the geometry and is a subset of a larger domain D. This situation is graphically represented by Fig. 2b.

2.2. Immersed isogeometric approach

The goal of the topology optimization is to find an optimal material distribution Ω under given constraints, such as boundary conditions or area penalization. This can be formulated as a minimization problem. In this scenario, the domain Ω changes during the optimization process, and solving the problem numerically would require redefining the mesh at each iteration. To avoid the necessity of remeshing, we formulate the problem on the fixed domain D, as shown in Fig. 2b, instead of Ω, shown in Fig. 2a, and we introduce a material property alpha, which is equal to α_{in} if it is inside Ω and a small value α_{out} for outside. This approach is based on immersed methods, which are extensively applied in fluid mechanics, solid mechanics, interface problems, and several other areas. An extensive explanation of immersed methods and their aspects can be found in [12, 41, 45]. In this way, this approach allows us to define which part of D represents Ω, so that the governing equations for the linear elasticity problem can be rewritten as:

$$\begin{cases} -\nabla\cdot(\alpha_\Omega\boldsymbol{\sigma}(\mathbf{u})) = \mathbf{0} & \text{in } D, \\ \mathbf{u} = \mathbf{0} & \text{on } \Gamma_D, \\ \boldsymbol{\sigma}(\mathbf{u})\cdot\mathbf{n} = \boldsymbol{\tau} & \text{on } \Gamma_N, \\ \boldsymbol{\sigma}(\mathbf{u})\cdot\mathbf{n} = \mathbf{0} & \text{on } \Gamma_0, \end{cases} \quad \text{with} \quad \alpha_\Omega = \begin{cases} \alpha_{\text{in}} & \text{in } \Omega, \\ \alpha_{\text{out}} & \text{on } D\setminus\overline{\Omega}, \end{cases} \tag{2}$$

where $\alpha_{\text{out}} \ll 1$ is a penalization parameter for the void, small enough to neglect the basis functions located outside the domain Ω, but not too small to result in an ill-conditioned stiffness matrix [33].

Therefore, to finally solve the problem numerically, we discretize the domain D using a background mesh, as shown in Fig. 2c, where the basis functions used to approximate the solution field are B-splines of degree p, refined from the geometry D. These basis functions are constructed from a non-decreasing set of coordinates called knot vector

$$\Xi = \{\xi_1, \xi_2, ..., \xi_{n+p}, \xi_{n+p+1}\} \tag{3}$$

defined in a parameter space $\mathbb{P} = [\xi_1, \xi_{n+p+1}]$ of B-splines, where n is the number of basis functions and p is the polynomial degree. This construction is defined recursively starting from piecewise constant functions for $p = 0$:

$$B_{i,0} = \begin{cases} 1 & \text{if } \xi_i \leq \xi < \xi_{i+1}, \\ 0 & \text{otherwise,} \end{cases} \tag{4}$$

and extended for higher degrees $p > 0$ by applying the Cox–de Boor formula [21]

$$B_{i,p} = \frac{\xi - \xi_i}{\xi_{i+p} - \xi_i} B_{i,p-1}(\xi) + \frac{\xi_{i+p+1} - \xi}{\xi_{i+p+1} - \xi_{i+1}} B_{i+1,p-1}(\xi). \tag{5}$$

In sequence, having the basis functions in each parametric direction, the geometry mapping from the parametric domain $\mathbb{P}^2 = [\xi_1, \xi_{n+p+1}] \times [\eta_1, \eta_{m+p+1}]$ to the physical domain $\mathbb{R}^2$ is then defined as

$$\mathbf{x}(\xi, \eta) = \sum_{i=1}^{n} \sum_{j=1}^{m} B_{i,p}(\xi) B_{j,p}(\eta) \mathbf{C}_{i,j}, \tag{6}$$

where $\mathbf{C}_{i,j}$ are the control points that define the geometry.

Note that the basis functions used to approximate the solution field may have a different polynomial degree p than those used to construct the geometry D. However, the geometric mapping remains based on the B-splines defined from the geometry D. Finally, the implementation of the problem is made within an open-source IGA code [43], which provides the necessary features.

2.3. Minimization problem

The minimization problem mentioned in the previous subsection, which defines the topology optimization process, has aims to find the optimal domain $\Omega \subset D$ that minimizes a cost function J. This expression can be written as:

$$\min_{\Omega \in \mathcal{E}} J(\Omega, \mathbf{u}), \tag{7}$$

where $\mathcal{E}$ is a set of admissible subsets of D, and

$$J(\Omega, \mathbf{u}) = \int_D \alpha_\Omega \boldsymbol{\sigma}(\mathbf{u}) : \boldsymbol{\epsilon}(\mathbf{u}) \, dD + l \int_\Omega \, d\Omega. \tag{8}$$

Note that the area constraint, which prevents the solution from being $\Omega = D$, is addressed by the second term of the objective function and is controlled by the parameter l [24].

3. Discretized level-set representation

The domain Ω is represented by a continuous level-set function. This means that the interface that divides the material region Ω from the void region $D \setminus \Omega$ is defined by the zero set of the level-set function. Specifically, all points where the level-set function is smaller than 0 belong to Ω, points where it is higher than zero belong to the void $D \setminus \Omega$, and points where the level-set function is equal to zero lie on the interface between the two regions:

$$\begin{cases} \phi(\mathbf{x}) < 0 & \iff \mathbf{x} \in \Omega, \\ \phi(\mathbf{x}) = 0 & \iff \mathbf{x} \in \partial\Omega, \\ \phi(\mathbf{x}) > 0 & \iff \mathbf{x} \in D \setminus \overline{\Omega}. \end{cases} \tag{9}$$

As the background mesh D is discretized, we also discretize the domain Ω. Therefore, the level-set discretization is made using B-spline basis functions of degree d, which might be the same or different from the degree p of the basis functions used for approximating the solution,

$$\phi(\xi, \eta) = \sum_{i=1}^{n} \sum_{j=1}^{m} B_{i,d}(\xi) B_{j,d}(\eta) c_{i,j}. \tag{10}$$

In sequence, the coefficients $c_{i,j}$ are obtained by solving a collocation problem, which enforces that the discretized level-set function (10) matches the initial level-set function at the Greville abscissas. The positions of the Greville abscissas, shown in Fig. 3, serve as anchors for the B-splines and are computed as

$$\widetilde{\xi}_i = \frac{\xi_{i+1} + \xi_{i+2} + ... + \xi_{i+d}}{d}, \qquad i = 1, ..., n. \tag{11}$$

During the optimization process, the evaluations of the level-set function at the Greville abscissas are updated, and the coefficients $c_{i,j}$ for the new level-set function discretization are obtained in the same process.

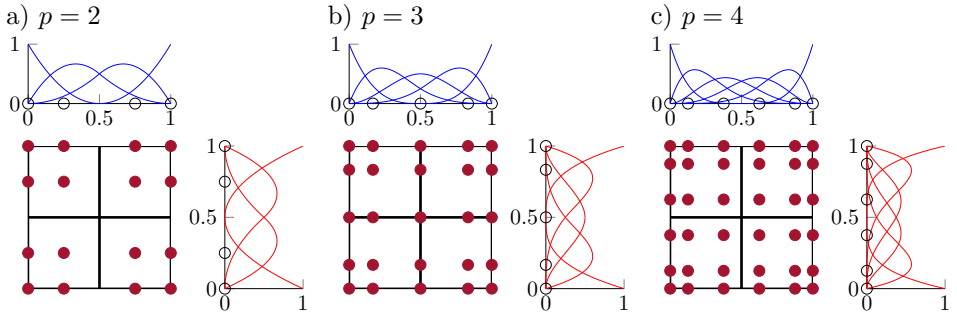

Fig. 3. Distribution of the Greville abscissae on the elements for different polynomial degrees, with basis functions defined as: a) $\Xi = \{0\,0\,0\,0.5\,1\,1\,1\}$, b) $\Xi = \{0\,0\,0\,0\,0.5\,1\,1\,1\,1\}$, c) $\Xi = \{0\,0\,0\,0\,0\,0.5\,1\,1\,1\,1\,1\,1\}$.

In Fig. 4, we observe the identification process of the region where the element is located. This is achieved by evaluating the level-set function at a set of points in each element. Then, based on the signs of these evaluations, we can identify the region of the element and assign the corresponding material property. For cut elements, the material property is computed as the average based on the cut ratio of the element, given by

$$\alpha|_T = \alpha_{\text{out}} + \frac{|T \cap \Omega|}{|T|}(\alpha_{\text{in}} - \alpha_{\text{out}}). \tag{12}$$

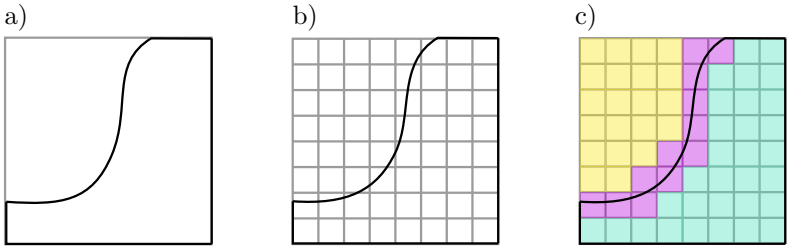

Fig. 4. Type identification of the elements for assembling the material property α: a) domain D divided into two regions by a level-set function, b) domains D discretized as the background mesh, c) identification of the elements; the elements outside Ω are in yellow, inside Ω in blue, and the cut elements in pink.

4. Topological derivatives

In the previous sections, we defined the representation of a fixed domain D and a level-set function ϕ used to represent the domain Ω, both discretized by B-splines. In the following, we discuss how the topological derivative is computed and how the level-set function is updated, focusing on minimizing the cost function.

Consider a point $\mathbf{x}_0 \in D \setminus \partial\Omega$, and define $\omega_\varepsilon(\mathbf{x}_o) = \{\mathbf{x} \in \mathbb{R}^2 : ||\mathbf{x}_0 - \mathbf{x}|| < \varepsilon\}$ as a circular perturbation of radius ε centered at $\mathbf{x}_0$. The introduction of the perturbation $\omega_\varepsilon(\mathbf{x}_o)$ in the domain D results in a perturbed domain:

$$\Omega_\varepsilon = \begin{cases} \Omega \setminus \overline{\omega_\varepsilon(\mathbf{x}_0)} & \text{if } \mathbf{x}_0 \in \Omega, \\ \Omega \cup \omega_\varepsilon(\mathbf{x}_0) & \text{if } \mathbf{x}_0 \in D \setminus \overline{\Omega}. \end{cases} \tag{13}$$

Let $\mathcal{J}(\Omega) := J(\Omega, \mathbf{u}(\Omega))$ denote the reduced cost function where $\mathbf{u}(\Omega)$ denotes the unique solution to (1) for a given subdomain Ω. In this scenario, to measure the change in the cost function J when a new hole around the point x_0 is introduced, the topological derivative is defined as

$$d\mathcal{J}(\Omega)(\mathbf{x}_0) := \lim_{\varepsilon \to 0} \frac{\mathcal{J}(\Omega_\varepsilon) - \mathcal{J}(\Omega)}{|\omega_\varepsilon|} = \lim_{\varepsilon \to 0} \frac{J(\Omega_\varepsilon, \mathbf{u}_\varepsilon) - J(\Omega, \mathbf{u})}{|\omega_\varepsilon|},$$

where $\mathbf{u}_\varepsilon$ is the solution of (1) with Ω replaced by Ω_ε.

To evaluate this expression, we adopt the approach proposed in [18], which introduces the Lagrangian

$$L(\Omega, \mathbf{u}, \boldsymbol{\lambda}) = J(\Omega, \mathbf{u}) + \boldsymbol{\lambda} E(\Omega, \mathbf{u}),$$

where $E(\Omega, \mathbf{u}) = 0$ represents the weak form of the governing equation. This implies that $L(\Omega, \mathbf{u}, \boldsymbol{\lambda}) = J(\Omega, \mathbf{u})$ at the solution for all $\boldsymbol{\lambda}$. Consequently, the topological derivative can be rewritten as

$$d\mathcal{J}(\Omega)(\mathbf{x}_0) = \lim_{\varepsilon \to 0} \frac{L(\Omega_\varepsilon, \mathbf{u}_\varepsilon, \boldsymbol{\lambda}) - L(\Omega, \mathbf{u}, \boldsymbol{\lambda})}{|\omega_\varepsilon|}. \tag{14}$$

By introducing in the adjoint state $\boldsymbol{\lambda}$ defined as the solution of $\partial_{\mathbf{u}} L(\Omega, \mathbf{u}, \boldsymbol{\lambda}) = 0$, and noting that $\boldsymbol{\lambda} = -\frac{1}{2}\mathbf{u}$, after solving this limit for the linear elasticity problem, as shown in [6], an analytical expression is obtained, which depends only on the solution $\mathbf{u}$ and the material coefficient α:

$$d\mathcal{J}(\Omega)(\mathbf{x}_0) = \begin{cases} d\mathcal{J}_{\text{in}}(\Omega)(\mathbf{x}_0) = -3\alpha_{\text{in}} \left(\dfrac{\alpha_{\text{out}} - \alpha_{\text{in}}}{2\alpha_{\text{out}} + \alpha_{\text{in}}} \right) \boldsymbol{\sigma}(\mathbf{u}) : \boldsymbol{\epsilon}(\mathbf{u}) - l \\ \qquad\qquad\qquad\qquad\qquad\qquad\qquad\qquad \text{if } \mathbf{x}_0 \in \Omega, \\ d\mathcal{J}_{\text{out}}(\Omega)(\mathbf{x}_0) = -3\alpha_{\text{out}} \left(\dfrac{\alpha_{\text{in}} - \alpha_{\text{out}}}{2\alpha_{\text{in}} + \alpha_{\text{out}}} \right) \boldsymbol{\sigma}(\mathbf{u}) : \boldsymbol{\epsilon}(\mathbf{u}) + l \\ \qquad\qquad\qquad\qquad\qquad\qquad\qquad\qquad \text{if } \mathbf{x}_0 \in D \setminus \overline{\Omega}. \end{cases} \tag{15}$$

From this, the generalized topological derivative is then defined as:

$$g_\Omega(\mathbf{x}) = \begin{cases} -d\mathcal{J}(\Omega)(\mathbf{x}) & \text{if } \mathbf{x} \in \Omega, \\ d\mathcal{J}(\Omega)(\mathbf{x}) & \text{if } \mathbf{x} \in D \setminus \overline{\Omega}, \end{cases} \tag{16}$$

and is used to update the level-set function, guiding the evolution of the domain Ω. Algorithm 1 shows this update process. The update of the level-set is guided under a spherical linear interpolation, which uses the angle θ_i, in the L^2-sense, between the current level-set ϕ_i and the topological derivative g_i, as a parameter to define the next domain Ω_{i+1}. Note that the stopping criterion is controlled by the same angle θ_i, and this quantity works as a comparison between the current topological derivative g_i and the level-set function ϕ_i. Then, if $\theta_i = 0$, the domain Ω_{i+1} is optimal and the topological derivative g_i can be used as the level-set function ϕ [7]. During this process, we apply a line search to define the parameter κ used to update the level-set in the spherical linear interpolation. Additional filtering processes are applied, described in Sec. 5, to smooth the generalized topological derivative g, working similarly to sensitivity filtering in density-based optimization [19].

Algorithm 1: Level-set update.

Initialize the level-set function ϕ_1;
for $i \leftarrow 1$ ***to*** $n_{\max}$ **do**
  Compute $g_{\Omega_i}(\mathbf{x}) = \begin{cases} -d\mathcal{J}(\Omega_i)(\mathbf{x}) & \text{if } \mathbf{x} \in \Omega_i \\ d\mathcal{J}(\Omega_i)(\mathbf{x}) & \text{if } \mathbf{x} \in D \setminus \overline{\Omega_i} \end{cases}$;
  Compute $\theta_i = \arccos\left(\dfrac{\langle \phi_i, g_{\Omega_i} \rangle}{||g_{\Omega_i}||_{L^2(D)} ||\phi_i||_{L^2(D)}}\right)$;
  if $\theta_i < \varepsilon_\theta$ **then**
    break;
  else
    $\phi_{i+1} = \dfrac{1}{\sin\theta_i}(\sin((1-\kappa_i)\theta_i)\phi_i + \sin(\kappa_i\theta_i)g_{\Omega_i})$,
    where $\kappa = \max\left\{1, \dfrac{1}{2}, \dfrac{1}{4}, ...\right\}$ such that $\mathcal{J}(\Omega_{i+1}) < \mathcal{J}(\Omega_i)$;
  end
  Update c_{ij} in the discretization $\phi(\xi,\eta) = \sum_{i=1}^{n}\sum_{j=1}^{m} B_{i,d}(\xi)B_{j,d}(\eta)c_{ij}$
end
return ϕ;

In the discretized setting, when an element e of the background mesh D is cut by the interface of the level-set function ϕ, the generalized topological derivative is computed using a linear interpolation between the values computed inside and outside the domain Ω, given by

$$g_\Omega|_e(\mathbf{x}) = d\mathcal{J}_{\text{out}}(\Omega)(\mathbf{x})|_e + \frac{|e \cap \Omega|}{|e|}(-d\mathcal{J}_{\text{in}}(\Omega)(\mathbf{x})|_e - d\mathcal{J}_{\text{out}}(\Omega)(\mathbf{x})|_e). \quad (17)$$

5. Cut elements

The correct integration of elements intersected by the level-set function as well as the precise assignment of the material parameter in these elements plays an important role in the quality of the results. Therefore, in this section, we present the procedures used to deal with the cut elements.

In the computation of the cut ratio $|e \cap \Omega|/|e|$, necessary to obtain the α property for the cut elements, we apply a quadrature library for implicitly defined geometries [31, 32]. This library precisely follows the level-set function and provides quadrature points conforming to its zero isoline, as we can see in Fig. 5a. This quadrature allows the integration of the regions defined by the zero level-set with high precision, even for complex geometries with high-degree representations of the interfaces. Therefore, with this quadrature, we can precisely capture the transition between the material property α in the inner and outer parts of the domain Ω. Some examples for area computation, moving geometries, and linear elasticity can be found in [39, 40].

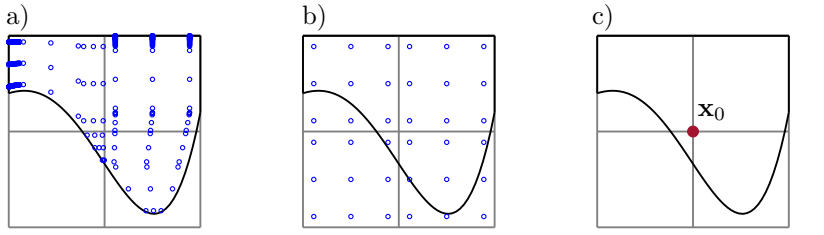

Fig. 5. Approaches to treat the cut elements: a) cut ratio computation, b) integration for assembly, c) average filtering.

However, when applying this precise quadrature rule for assembly, we obtain some instabilities in the shape due to the integration of small parts of basis functions located in regions defined by the level-set function, as well as to the jump between material and void regions, which results in a discontinuous field $\mathbf{u}$ and is approximated with higher-degree basis functions. To smooth these results, in the assembly process, we use the standard Gauss quadrature over the whole cut element and scale the local contribution by the corresponding material property α, computed using the aforementioned procedure, shown in Fig. 5b. Therefore, this approach smooths out the discontinuity in the transition between the elements and results in a solution with less numerical noise.

Another smoothing step may be applied to the generalized topological derivative. In particular, since we define an α property at each element, it occurs that, when evaluating the derivative at a Greville point, shared by multiple elements, as we can see in Fig. 5c, we have more than one α at the point. And to solve

this, we consider the average of the derivative around that point. This procedure effectively creates a smooth transition where the material property changes and works well as a sensitivity filter [17].

A second filtering step to smooth the generalized topological derivative g is performed by replacing g in the spherical linear interpolation, as described in Algorithm 1, using the solution $\widetilde{g}$ of the PDE:

$$\begin{aligned} -\gamma\Delta\widetilde{g}_\Omega + \widetilde{g}_\Omega &= g_\Omega \quad \text{in } D, \\ \nabla\widetilde{g}_\Omega \cdot \mathbf{n} &= 0 \qquad \text{on } \partial D. \end{aligned} \tag{18}$$

6. Numerical results

In this section, two numerical results for different geometries are presented. In both examples, the level-set is initialized as $\phi(\mathbf{x}) = -1$, which results in a full material background mesh, and the background mesh is discretized with 128×128 elements. The material coefficients used are $\alpha_{\text{in}} = 1$ for the material region Ω and $\alpha_{\text{out}} = 10^{-4}$ for the void region $D \setminus \overline{\Omega}$. Additionally, the parameter for area control is $l = 5$, the size control coefficient for the filtering is $\gamma = 10^{-4}$, and the Young modulus and the Poisson ratio are 1 and 1/3, respectively. In these examples, we investigate the sensitivity of the level-set function representation by applying different polynomial degrees d for the level-set function discretization and p for approximating the solution. This is done considering two settings: one with the level-set function and the solution both approximated with the same polynomial degree, and another with a linear level-set function representation combined with a higher-degree approximation of the solution. For the optimization algorithm, we consider a tolerance of $\varepsilon_\theta = 1$ and a maximum number of iterations of 200.

6.1. Cantilever

The first example is the cantilever problem, a benchmark example for topology optimization present in a large number of research papers (see, e.g., [2–4, 7, 22–24, 30, 35]). In our case, the domain D is represented by the mapping from the parameter domain $\hat{D} = [0, 1] \times [0, 1]$ to a rectangle of size 2×1 with homogeneous Dirichlet boundary conditions on the left and a concentrated load on the right, as shown in Fig. 6a. Figure 6b shows the final design for $p = d = 2$, and Fig. 7 shows the evolution of the cost function, angle, and area for the two settings. Additionally, the final shapes for different configurations of polynomial degree for the solution and the level-set function discretization are shown in Fig. 8. A mesh sensitivity study with 32×32, 64×64, 128×128 and 256×256 elements is presented in Figs. 9 and 10.

These results show that higher polynomial degrees p provide better convergence behavior compared to $p = 1$, with a faster drop in the middle region of

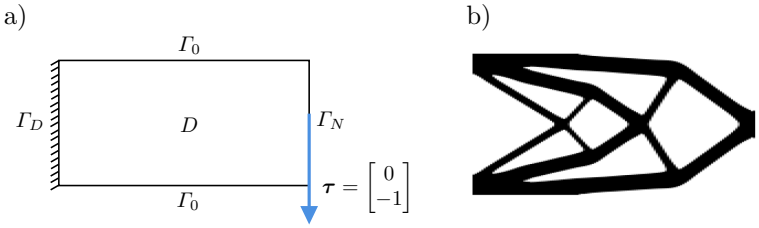

FIG. 6. Cantilever problem: a) initial problem, b) final shape.

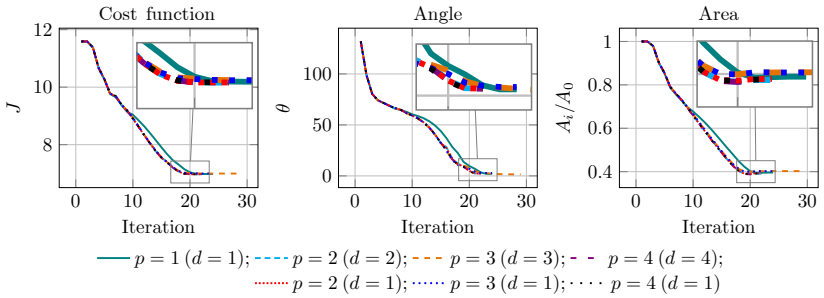

FIG. 7. Comparison of the evolution of the cost function, angle, and area for different polynomial degrees of solution approximation, with a linear level-set function representation (dotted), and with a level-set function representation with the same polynomial degree as the solution approximation (dashed).

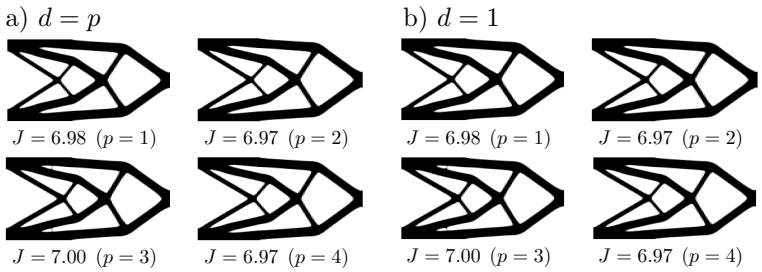

FIG. 8. Final shape for different basis function degrees used for approximating the solution: a) level-set function discretized with the same polynomial degree as the solution, b) level-set function discretized with linear basis functions.

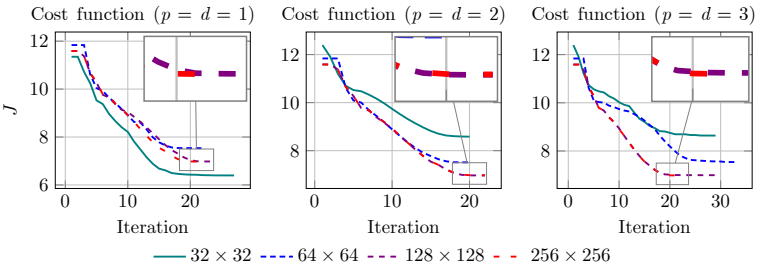

FIG. 9. Comparison of the evolution of the cost function for different mesh resolutions, using the same polynomial degrees for solution approximation and level-set function representation.

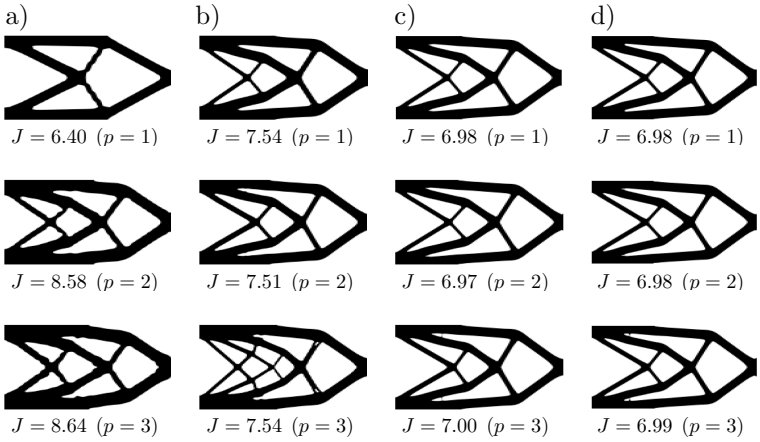

Fig. 10. Final shapes for $p = d$ and meshes using different numbers of elements per direction: a) 32×32, b) 64×64, c) 128×128, d) 256×256.

the graph in Fig. 7. However, since we use a fine mesh (128×128) to accurately represent the topology of the shape, increasing the polynomial degree p does not necessarily improve the accuracy of the solution. In addition, in all cases for this fine mesh, we converge to the same final solution (shown in Fig. 8), with similar convergence paths for higher degrees p, and the same number of steps is required for $p = 2$ and $p = 4$ in both level-set discretization settings, see Fig. 7. However, when using $p = 3$, 29 steps are required for the higher-degree level-set discretization ($d = p$), compared to 24 steps for the linear level-set discretization ($d = 1$). We also observe a slight difference in the final part of the area graph between different solution discretizations using odd and even B-spline degrees. This difference happens because, in the Greville abscissae for odd degrees, some points are shared between elements. As a result, averaging is performed around these positions when evaluating the solution, effectively acting as a filtering process [17]. While this helps to smooth the solution, it introduces a small difference compared to cases where such averaging is not required.

Figures 9 and 10 show the impact of the background mesh resolution on the final shape. As our optimization problem is not convex, it is reasonable to expect different topologies for different mesh sizes (e.g., Fig. 10a for $p = d = 1$, and Fig. 10b for $p = d = 3$). For $p = d = 2$, however, similar final topologies are obtained for all different mesh sizes. In addition, since we can represent the design more accurately with decreasing mesh size (i.e., the design space increases), we are able to find better local minima with decreasing function values from 8.58 (Fig. 10a, $p = d = 2$) to 6.97 (Fig. 10c, $p = d = 2$). Comparing the results using our standard mesh (128×128, Fig. 10c) to the finest one (256×256, Fig. 10d), we observe the same designs with minor variations in the objective value for all polynomial degrees. In Fig. 9, the evolutions of the cost functional for $p = d = 2$

and $p = d = 3$ on the 128×128 and 256×256 meshes are identical. This demonstrates that our method is mesh-independent, i.e., stable with respect to further mesh refinements, with the minimal feature size determined by the filtering of the topological derivative (18).

6.2. Quarter ring

This example has also been considered in several research papers [4, 5, 14, 22], where the same geometry is applied under different approaches and loading configurations. In our example, the domain D is defined by a mapping from the parameter domain $\widehat{D} = [0,1] \times [0,1]$ to a quarter ring of inner radius $R_{\text{in}} = 1$ and outer radius $R_{\text{out}} = 2$. Homogeneous Dirichlet boundary conditions are imposed on the bottom boundary, and a concentrated load is applied at $(0, 2)$, as illustrated in Fig. 11a. The final design for $p = d = 3$ is shown in Fig. 11b, while the evolution of the level-set function and the corresponding final shapes are presented in Figs. 12 and 13, respectively.

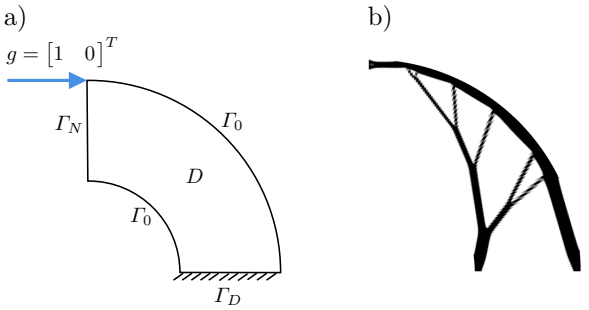

FIG. 11. Curved cantilever problem: a) initial problem, b) final shape.

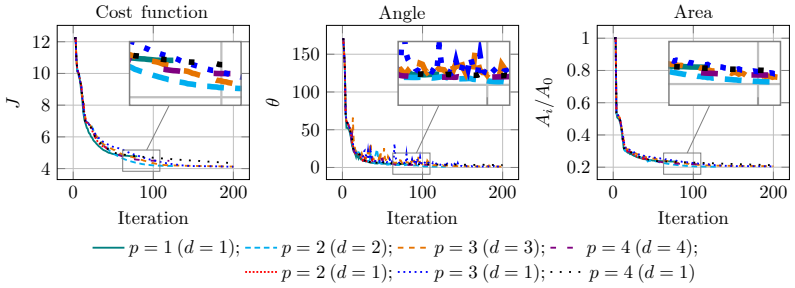

FIG. 12. Comparison of the evolution of the cost function, angle, and area for different polynomial degrees of solution approximation, with a linear level-set function representation (dotted), and with a level-set function representation with the same polynomial degree as the solution approximation (dashed).

From these results, we observe that for $p = 1$ $(d = 1)$ and $p = 2$ $(d = 1)$ the optimization stops after 80 and 43 iterations, with angles θ equal to 4.72 and 9.33, respectively, while in all of the remaining simulations an angle $\theta < 4$

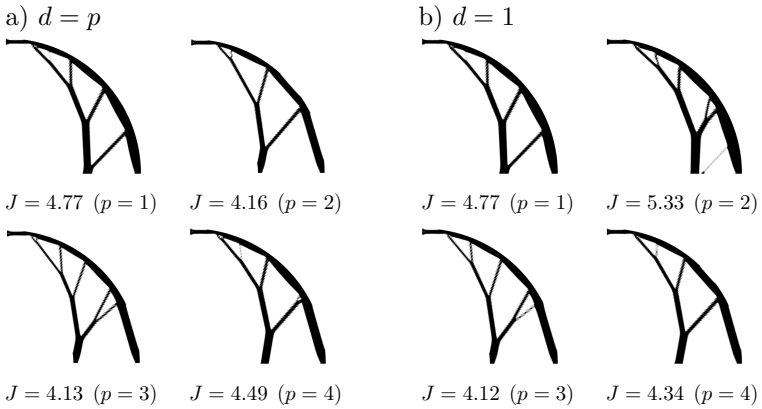

Fig. 13. Final shape for different basis function degrees used for approximating the solution: a) level-set function discretized with the same polynomial degree as the solution, b) level-set function discretized with linear basis functions.

is reached, which is a reasonable value for a numerical solutions [7]. We also notice that, although the cost function converges to a similar minimum value, all the shapes present different solutions with different configurations of features. Regarding the minimization, the lowest cost function values are obtained for $p = 3$ $(d = 1)$ with 4.12 and $p = 3$ $(d = 3)$ with 4.13, both achieved in 200 iterations. While, for $p = 2$ $(d = 2)$, a slightly higher value of 4.15 is obtained, but it requires only 129 iterations.

In topology optimization, the presence of a local minimum is a well-known challenge and depends on the choice of initial parameters [37]. Small variations in the definition of the initial setting of parameters can lead to different solutions. As a result, even if the initialization is too far from the global minimum, we still can achieve a solution that converges to a local minimum [3]. Therefore, while strategies such as refining the mesh in a coarse-to-fine approach can partially cure this issue, they do not eliminate it [1]. In this example, we notice that the possibility of setting different configurations of polynomial degrees for the level-set discretization and solution approximation, does not overcome this phenomenon completely. However, depending on the choice of setting, we can obtain a solution that satisfies the condition of having a small θ. Another parameter that can be changed and opens the possibility to find different solutions is the parameter γ, which limits the size of features in the filtering process, overcoming some noise in the final shape.

7. Conclusion

In this work, we developed an immersed isogeometric approach for level-set-based topology optimization guided only by the topological derivative. The

isogeometric approach within this framework provides seamless geometry update through a simplified meshing process, defined by a knot vector and control points. It also facilitates straightforward higher-order simulations, yielding results that are comparable to or slightly better than those obtained by standard approaches. In addition, the elements cut by the level-set function are treated using a quadrature library for implicitly defined geometries to compute a material property used to neglect the contributions from outside the domain Ω. A filtering process is also applied to material values to smooth changes between elements.

This study investigated the impact of using higher-degree basis functions for both the approximation of the solution and the discretization of the level-set function. In this investigation, we observed that being able to perform higher-order simulations can be beneficial in terms of iterations or final cost function values. However, regarding the level-set discretization, we observe that using linear basis functions yields results comparable to those obtained with higher-degree polynomials. Therefore, although the level-set is continuous, there is a discontinuity in the material property between the material region and the void. Our results indicate that using higher-degree basis functions does not directly imply a better representation of the jump across the interface. We will further investigate this aspect in future research. In addition, the proposed approach is currently limited to single-patch background geometries, and extending it to multi-patch structures is also a subject for future research.

Acknowledgements

This work wais supported by the joint DFG/FWF Collaborative Research Centre CREATOR (CRC – TRR361/F90; Grant-DOI 10.55776/F90) at TU Darmstadt, TU Graz, RICAM and JKU Linz. Moreover, P. G. is partially supported by the State of Upper Austria.

References

1. Allaire G., Jouve F., Coupling the level set method and the topological gradient in structural optimization, [in:] *Proceedings IUTAM Symposium on Topological Design Optimization of Structures, Machines and Materials*, pp. 3–12, Dordrecht, 2006, https://doi.org/10.1007/1-4020-4752-5_1.

2. Allaire G., Jouve F., Toader A., A level-set method for shape optimization, *Comptes Rendus. Mathématique*, **334**(12): 1125–1130, 2002, https://doi.org/10.1016/S1631-073X(02)02412-3.

3. Allaire G., Jouve F., Toader A., Structural optimization using sensitivity analysis and a level-set method, *Journal of Computational Physics*, **194**(1): 363–393, 2004, https://doi.org/10.1016/j.jcp.2003.09.032.

4. Aminzadeh M., Tavakkoli S.M., A parameter space approach for isogeometrical level set topology optimization, *International Journal for Numerical Methods in Engineering*, **123**(15): 3485–3506, 2022, https://doi.org/10.1002/nme.6976.

5. Aminzadeh M., Tavakkoli S.M., Multiscale topology optimization of structures by using isogeometrical level set approach, *Finite Elements in Analysis and Design*, **235**: 104167, 2024, https://doi.org/10.1016/j.finel.2024.104167.

6. Amstutz S., Sensitivity analysis with respect to a local perturbation of the material property, *Asymptotic Analysis*, **49**(1–2): 87–108, 2006, https://doi.org/10.3233/ASY-2006-778.

7. Amstutz S., Andrä H., A new algorithm for topology optimization using a level-set method, *Journal of Computational Physics*, **216**(2): 573–588, 2006, https://doi.org/10.1016/j.jcp.2005.12.015.

8. Amstutz S., Novotny A.A., de Souza Neto E.A., Topological derivative-based topology optimization of structures subject to Drucker–Prager stress constraints, *Computer Methods in Applied Mechanics and Engineering*, **233–236**: 123–136, 2012, https://doi.org/10.1016/j.cma.2012.04.004.

9. Bends?e M.P., Kikuchi N., Generating optimal topologies in structural design using a homogenization method, *Computer Methods in Applied Mechanics and Engineering*, **71**(2): 197–224, 1988, https://doi.org/10.1016/0045-7825(88)90086-2.

10. Burger M., Hackl B., Ring W., Incorporating topological derivatives into level set methods, *Journal of Computational Physics*, **194**(1): 344–362, 2004, https://doi.org/10.1016/j.jcp.2003.09.033.

11. Carvalho F.S., Ruscheinsky D., Giusti S.M., Anflor C.T.M., Novotny A.A., Topological derivative-based topology optimization of plate structures under bending effects, *Structural and Multidisciplinary Optimization*, **63**: 617–630, 2021, https://doi.org/10.1007/s00158-020-02710-4.

12. de Prenter F., Verhoosel C.V., van Brummelen E.H., Larson M.G., Badia S., Stability and conditioning of immersed finite element methods: Analysis and remedies, *Archives of Computational Methods in Engineering*, **30**: 3617–3656, 2023, https://doi.org/10.1007/s11831-023-09913-0.

13. Deaton J.D., Grandhi R.V., A survey of structural and multidisciplinary continuum topology optimization: Post 2000, *Structural and Multidisciplinary Optimization*, **49**: 1–38, 2014, https://doi.org/10.1007/s00158-013-0956-z.

14. Dedé L., Borden M.J., Hughes T.J.R., Isogeometric analysis for topology optimization with a phase field model, *Archives of Computational Methods in Engineering*, **19**: 427–465, 2012, https://doi.org/10.1007/s11831-012-9075-z.

15. Feppon F., Allaire G., Dapogny C., Jolivet P., Body-fitted topology optimization of 2D and 3D fluid-to-fluid heat exchangers, *Computer Methods in Applied Mechanics and Engineering*, **376**: 113638, 2021, https://doi.org/10.1016/j.cma.2020.113638.

16. Luz Filho J.M.M., Mattoso R., Fernandez L., A freeFEM code for topological derivative-based structural optimization, *Structural and Multidisciplinary Optimization*, **66**: 74, 2023, https://doi.org/10.1007/s00158-023-03529-5.

17. Gangl P., A multi-material topology optimization algorithm based on the topological derivative, *Computer Methods in Applied Mechanics and Engineering*, **366**: 113090, 2020, https://doi.org/10.1016/j.cma.2020.113090.

18. Gangl P., Sturm K., A simplified derivation technique of topological derivatives for quasi-linear transmission problems, *ESAIM – Control, Optimisation and Calculus of Variations*, **26**: 106, 2020, https://doi.org/10.1051/cocv/2020035.

19. Gangl P., Komann T., Krenn N., Ulbrich S., Robust topology optimization of electric machines using topological derivatives, *Arxiv*, 2025, http://arxiv.org/abs/2504.05070.

20. Gao J., Xiao M., Zhang Y., Gao L., A comprehensive review of isogeometric topology optimization: Methods, applications and prospects, *Chinese Journal of Mechanical Engineering*, **33**: 87, 2020, https://doi.org/10.1186/s10033-020-00503-w.

21. Hughes T.J.R., Cottrell J.A., Bazilevs Y., Isogeometric analysis: CAD, finite elements, NURBS, exact geometry and mesh refinement, *Computer Methods in Applied Mechanics and Engineering*, **194**(39–41): 4135–4195, 2005, https://doi.org/10.1016/j.cma.2004.10.008.

22. Jahangiry H.A., Tavakkoli S.M., An isogeometrical approach to structural level set topology optimization, *Computer Methods in Applied Mechanics and Engineering*, **319**: 240–257, 2017, https://doi.org/10.1016/j.cma.2017.02.005.

23. Khatibinia M., Roodsarabi M., Structural topology optimization based on hybrid of piecewise constant level set method and isogeometric analysis, *International Journal of Optimization in Civil Engineering*, **10**(3): 493–512, 2020, https://www.researchgate.net/publication/342924423.

24. Krenn N., *Multi-Material Topology Optimization Subject to Pointwise Stress Constraints for Additive Manufacturing*, Master's Thesis, Graz University of Technology, 2021.

25. Lopes C.G., dos Santos R.B., Novotny A.A., Topological derivative-based topology optimization of structures subject to multiple load-cases, *Latin American Journal of Solids and Structures*, **12**(5): 834–860, 2015, https://doi.org/10.1590/1679-78251252.

26. Ma B., Zheng J., Lei G., Zhu J., Jin P., Guo Y., Topology optimization of ferromagnetic components in electrical machines, *IEEE Transactions on Energy Conversion*, **35**(2): 786–798, 2020, https://doi.org/10.1109/TEC.2019.2960519.

27. de Souza Neto E.A., Amstutz S., Giusti S.M., Novotny A.A., Topological derivative-based optimization of micro-structures considering different multi-scale models, *Computer Modeling in Engineering & Sciences*, **62**(1): 23–54, 2010, https://doi.org/10.3970/cmes.2010.062.023.

28. Novotny A.A., Lopes C.G., Santos R.B., Topological derivative-based topology optimization of structures subject to self-weight loading, *Structural and Multidisciplinary Optimization*, **63**: 1853–1861, 2021, https://doi.org/10.1007/s00158-020-02780-4.

29. Osher S., Sethian J.A., Fronts propagating with curvature-dependent speed: Algorithms based on Hamilton-Jacobi formulations, *Journal of Computational Physics*, **79**(1): 12–49, 1988, https://doi.org/10.1016/0021-9991(88)90002-2.

30. Roodsarabi M., Khatibinia M., Sarafrazi S.R., Hybrid of topological derivative-based level set method and isogeometric analysis for structural topology optimization, *Steel and Composite Structures*, **21**(6): 1389–1410, 2016, https://doi.org/10.12989/scs.2016.21.6.1389.

31. Saye R.I., High-order quadrature methods for implicitly defined surfaces and volumes in hyperrectangles, *SIAM Journal on Scientific Computing*, **37**(2): A993–A1019, 2015, https://doi.org/10.1137/140966290.

32. Saye R.I., High-order quadrature on multi-component domains implicitly defined by multivariate polynomials, *Journal of Computational Physics*, **448**: 110720, 2022, https://doi.org/10.1016/j.jcp.2021.110720.

33. Schillinger D., Ruess M., The finite cell method: A review in the context of higher-order structural analysis of CAD and image-based geometric models, *Archives of Computational Methods in Engineering*, **22**: 391–455, 2015, https://doi.org/10.1007/s11831-014-9115-y.

34. Shakour E., Amir O., Topology optimization with precise evolving boundaries based on IGA and untrimming techniques, *Computer Methods in Applied Mechanics and Engineering*, **374**: 113564, 2021, https://doi.org/10.1016/j.cma.2020.113564.

35. Shojaee S., Mohamadian M., Valizadeh N., Composition of isogeometric analysis with level set method for structural topology optimization, *International Journal of Optimization in Civil Engineering*, **2**(1): 47–70, 2012, https://www.researchgate.net/publication/259593893.

36. Sigmund O., Maute K., Topology optimization approaches: A comparative review, *Structural and Multidisciplinary Optimization*, **48**: 1031–1055, 2013, https://doi.org/10.1007/s00158-013-0978-6.

37. Sigmund O., Petersson J., Numerical instabilities in topology optimization: A survey on procedures dealing with checkerboards, mesh-dependencies and local minima, *Structural Optimization*, **16**: 68–75, 1998, https://doi.org/10.1007/BF01214002.

38. Suttakul P., Ngo H.T., Nguyen M.N., Bui T.Q., Rungamornrat J., Vo D., Isogeometric proportional topology optimization (IGA-PTO) for multi-material problems, *Mechanics of Advanced Materials and Structures*, **32**(20): 5006–5025, 2025, https://doi.org/10.1080/15376494.2024.2418352.

39. Teixeira G.H., Loibl M., Marussig B., Comparison of integration methods for cut elements, [in:] *Proceedings The 9th European Congress on Computational Methods in Applied Sciences and Engineering*, pp. 1–9, Lisboa, Portugal, 2024, https://doi.org/10.23967/eccomas.2024.098.

40. Toprak T. *et al.*, Employing continuous integration inspired workflows for benchmarking of scientific software – a use case on numerical cut cell quadrature, *Advances in Engineering Software*, **213**: 104087, 2026, https://doi.org/10.1016/j.advengsoft.2025.104087.

41. Verzicco R., Immersed boundary methods: Historical perspective and future outlook, *Annual Review of Fluid Mechanics*, **55**: 129–155, 2023, https://doi.org/10.1146/annurev-fluid-120720-022129.

42. Vo D., Nguyen M.N., Bui T.Q., Suttakul P., Rungamornrat J., Isogeometric gradient-free proportional topology optimization (IGA-PTO) for compliance problem, *International Journal for Numerical Methods in Engineering*, **124**(19): 4275–4310, 2023, https://doi.org/10.1002/nme.7315.

43. Vázquez R., A new design for the implementation of isogeometric analysis in Octave and MATLAB: Geopdes 3.0, *Computers and Mathematics with Applications*, **72**(3): 523–554, 2016, https://doi.org/10.1016/j.camwa.2016.05.010.

44. Wang M.Y., Wang X., Guo D., A level set method for structural topology optimization, *Computer Methods in Applied Mechanics and Engineering*, **192**(1–2): 227–246, 2003, https://doi.org/10.1016/S0045-7825(02)00559-5.

45. Wang X.S., Zhang L.T., Liu W.K., On computational issues of immersed finite element methods, *Journal of Computational Physics*, **228**(7): 2535–2551, 2009, https://doi.org/10.1016/j.jcp.2008.12.012.

46. Wiesheu M., Komann T., Merkel M., Schöps S., Ulbrich S., Cortes Garcia I., Combined parameter and shape optimization of electric machines with isogeometric analysis, *Optimization and Engineering*, **26**: 1011–1038, 2025, https://doi.org/10.1007/s11081-024-09925-0.

47. Xavier M., Novotny A.A., Topological derivative-based topology optimization of structures subject to design-dependent hydrostatic pressure loading, *Structural and Multidisciplinary Optimization*, **56**: 47–57, 2017, https://doi.org/10.1007/s00158-016-1646-4.

Received June 25, 2025; revised January 12, 2026; accepted January 17, 2026; available online January 20, 2026; version of record March 23, 2026.